Available online at www.sciencedirect.com
ScienceDirect
International Journal of Heat and Mass Transfer 50 (2007) 381–390
International Journal of HEAT and MASS TRANSFER
www.elsevier.com/locate/ijhmt

Heat transfer enhancement of Taylor–Couette–Poiseuille flow in an annulus by mounting longitudinal ribs on the rotating inner cylinder

Tzer-Ming Jeng [a,*], Sheng-Chung Tzeng [b], Chao-Hsien Lin [b]

[a] Department of Mechanical Engineering, Air Force Institute of Technology, Gangshan 820, Taiwan, ROC
[b] Department of Mechanical Engineering, ChienKuo Technology University, Changhua 500, Taiwan, ROC

Received 2 October 2005; received in revised form 10 June 2006
Available online 8 August 2006

Abstract

This work experimentally investigates the heat transfer characteristics of Taylor–Couette–Poiseuille flow in an annular channel by mounting longitudinal ribs on the rotating inner cylinder. The ranges of the axial Reynolds number (*Re*) and the rotational Reynolds number (Re_Ω) are $Re = 30$–1200 and $Re_\Omega = 0$–2922, respectively. Three modes of the inner cylinder without/with longitudinal ribs are considered. A special entry and exit design for the axial coolant flow reveals some interesting findings. The value of Nusselt number (*Nu*) is almost minimal at the inlet of the annular channel, and then sharply rises in the axial direction. The average Nusselt number ($\overline{Nu}$) increases with *Re*. *Nu* increases rapidly with Re_Ω at low *Re* (such as at $Re = 30$ and 60) but that the effect of Re_Ω decreases as the value increases (such as at $Re = 300$–1200). The ratio $\overline{Nu}/\overline{Nu}_0$ increases with Re_Ω and exceed two at all *Re* and in the test modes. The heat transfer is typically promoted by mounting longitudinal ribs on the rotating inner cylinder, especially at $Re = 300$ and 600. When $Re = 300$ or 600 and $Re_\Omega > 2000$, the $\overline{Nu}$ of the system with ribs reaches around 1.4 times that of $\overline{Nu}_A$ ($\overline{Nu}$ in mode A). Under a given pumping power constraint (PRe^3), the $\overline{Nu}$ of the system with ribs (modes B and C) generally exceeds that without ribs (mode A), while the difference between the values of $\overline{Nu}$ in modes B and A slowly falls as PRe^3 increases. Additionally, mode B (with ribs) is preferred for high heat transfer when $PRe^3 < 4.5 \times 10^{13}$ but mode C (with cavities on ribs) is optimal for high heat transfer when $PRe^3 > 4.5 \times 10^{13}$.

Keywords: Heat transfer; Taylor–Couette–Poiseuille flow; Longitudinal ribs; Rotating

1. Introduction

Many engineering applications involve rotating machinery components. They include rotating membrane filters, co-axial rotating heat pipes, rotating extractors, cylindrical bearings, and rotating power transmission systems [1–5]. A basic configuration for rotating machinery components is the annulus with a stationary outer cylinder and a rotating inner cylinder. The flow in such an annulus is called Taylor–Couette flow, in which the famous Taylor vortices appear when the rotational speed exceeds a critical value. These Taylor vortices (or the stability of the flow) have been studied extensively. These investigations [6–10] demonstrated the effects of the centrifugal force and the Coriolis force on the flow characteristics and showed that the following five dynamical transitions occur in the following order, as the rotational speed is slowly increased; laminar Couette flow → laminar Taylor vortex flow → wavy vortex flow → quasi-periodic wavy vortex flow → weakly turbulent wavy vortex flow → turbulent vortex flow. Additionally, the combination of Taylor–Couette flow and axial flow (Taylor–Couette–Poiseuille flow) has motivated many studies. Some works [11–13] have examined the generation and evolution of the vortex flow and have shown the

* Corresponding author. Tel.: +886 7 6256040; fax: +886 4 7357193.
E-mail addresses: tm.jeng@msa.hinet.net, t_m_jeng@yahoo.com.tw (T.-M. Jeng).

0017-9310/$ - see front matter © 2006 Elsevier Ltd. All rights reserved.
doi:10.1016/j.ijheatmasstransfer.2006.06.005

Nomenclature

L	length of the inner cylinder (m)
Nu	local Nusselt number, Eq. (5)
Pr	Prandtl number of fluid
q	wall heat flux (W/m^2)
r_i	radius of the inner cylinder (m)
r_o	radius of the outer cylinder (m)
Re	axial Reynolds number, Eq. (2)
Re_e	effective Reynolds number, Eq. (8)
Re_Ω	rotational Reynolds number, Eq. (3)
T_b	fluid bulk temperature (°C)
T_w	wall temperature (°C)
Ta	Taylor number, Eq. (1)
V_a	average axial velocity through the annular channel without ribs (m/s)
z	axial coordinate (m)

Greek symbols

μ	viscosity (kg/m s)
ρ	fluid density (kg/m^3)
Ω	rotational speed of the inner cylinder (rad./s)

Superscript

–	average

Subscript

0	stationary state

damping effect of the imposed axial flow on the internal motions of the vortices.

Excessive thermal stress can damage rotating machinery components. This fact has motivated numerous interesting studies on the mechanism of heat transfer in Taylor–Couette flow or Taylor–Couette–Poiseuille flow. Becker and Kaye [14] analyzed the effect of the radial temperature gradient on the stability of Taylor–Couette flow. They found that heating the inner rotating cylinder stabilizes the flow, while heating the outer stationary cylinder destabilizes it. They also plotted the Nusselt number against the Taylor number. The Taylor number is defined as

$$Ta = \frac{\rho^2\Omega^2[(r_o + r_i)/2](r_o - r_i)^3}{\mu^2} \tag{1}$$

Their data showed that the Nusselt numbers remained constant until the Taylor number exceeded a critical value, at which the Taylor vortices appear, beyond which they increased with Taylor numbers. Hayase et al. [15] numerically studied convective heat transfer in Taylor–Couette flow with periodically embedded cavities on the outer surface of the inner cylinder or on the inner surface of the outer cylinder. Their three-dimensional calculations indicated how the flow in a cavity interacts with Taylor vortices in the annular space to enhance heat transfer. Embedding cavities into the inner cylinder increases the transport of heat by a factor of 1.2 and embedding cavities into the outer cylinder increases the transport of heat by a factor of 1.1, relative to the heat transfer in the case with coaxial cylinders with smooth surfaces. Gardiner and Sabersky [16] measured the heat transfer coefficients in the Taylor–Couette problem with superimposed axial flow. The effects of the Taylor number, the axial Reynolds number and the Prandtl number on the heat transfer were elucidated. Their tests involved two rotors. One had a smooth surface, and the other had 30 longitudinal slots. Their data revealed that the heat transfer coefficients were normally higher in the latter case . They also reported that the motion of Taylor vortices decayed as the axial Reynolds number increased. These results are consistent with those of Simmers and Coney [17]. These researchers developed a Reynolds analogy solution to determine the heat transfer characteristics of combined Taylor vortices and axial flows. Lee and Minkowycz [18] measured the mass transfer of naphthalene to determine the heat transfer coefficients in a Taylor–Couette–Poiseuille problem. In their tests, the surfaces of the cylinders that comprised the annuli were either smooth or one was smooth and the other was grooved parallel to the axis. They found that the Nusselt number increased with the axial Reynolds number at low Taylor numbers but that the axial Reynolds number fell as the Taylor number continues to increase. Additionally, a critical Taylor number exists for a given axial Reynolds number, beyond which the Nusselt number increases sharply. Jakoby et al. [19] measured the flow field in the Taylor–Couette–Poiseuille flow using a time-dependent laser Doppler anemometer (LDA) and obtained the heat transfer from the hot gas to the rotating inner cylinder by a steady-state method. They produced a stability map to describe the evaluation of secondary Taylor-vortex flows based on the interactions between the Taylor–Couette flow and the axial flow. They also presented the relationship between the Nusselt number and the effective Reynolds number. The cited investigations have improved our understanding of the heat transfer mechanism in Taylor–Couette flow and Taylor–Couette–Poiseuille flow. Some have suggested the use of longitudinal cavities, slots, grooves or ribs in the annulus to promote heat transfer.

This work experimentally investigates the heat transfer characteristics of Taylor–Couette–Poiseuille flow in an annular channel by mounting longitudinal ribs on the rotating inner cylinder. Unlike in the literature, herein, three cavities were cut on the top surface of each longitudinal rib. This is a new configuration. As far as the authors know, the thermal performance of this configuration has not been studied. Additionally, the presented system has a specially designed entry and exit for axial coolant flow in practical applications (for example, in the rotary blade coupling of a four-wheel-drive vehicle). The axial coolant enters the front shield of the annulus through four inlet holes, and flows from the rear shield of the annulus through five outlet holes. These side shields affect the fluid flow characteristics. Therefore, the pertinent thermal behaviors in such a system are of great interest. Various axial Reynolds numbers and rotational Reynolds numbers are considered in the experiments conducted in this work. The results obtained herein indicate that the modified configuration with cavities on the ribs has potential in cooling the rotating machinery components.

2. Experimental apparatus and test section

The experimental apparatus presented in Fig. 1 was designed for measuring the heat transfer coefficient from the rotating inner cylinder to the air in the annular channel with axial air flow. The apparatus comprised four main parts: 1. rotating system; 2. test section; 3. data acquirement system, and 4. air supply system. The rotating system employed a 5 HP AC induction motor that drove the rotating shaft using a belt pulley system. The rate of rotation could be adjusted using an inverter to a maximum of 2000 RPM. Rates of rotation of 0, 73, 103, 230, 325, 727 and 1028 RPM were tested. The rate of rotation was measured using a photo-electronic tachometer. The assembly of the rotating system and the test section was dynamically balanced. The test section had a rotational inner cylinder and a stationary outer housing. The inner cylinder with a length of 120 mm and an outer diameter of 120 mm was made of 40 mm-thick Teflon. Teflon has a very low conductivity and can reduce heat loss through the inner cylinder. The outer housing, made of 20 mm-thick aluminum alloy, consisted of three parts: 1. front shield; 2. outer cylinder, and 3. rear shield. The outer cylinder was 165 mm long and had a diameter of 134 mm. The inner-cylinder configuration had three test modes, as shown in Fig. 3. Mode A involved an inner cylinder with a smooth outer surface. In modes B and C, four longitudinal aluminum ribs were periodically mounted on the outer surface of

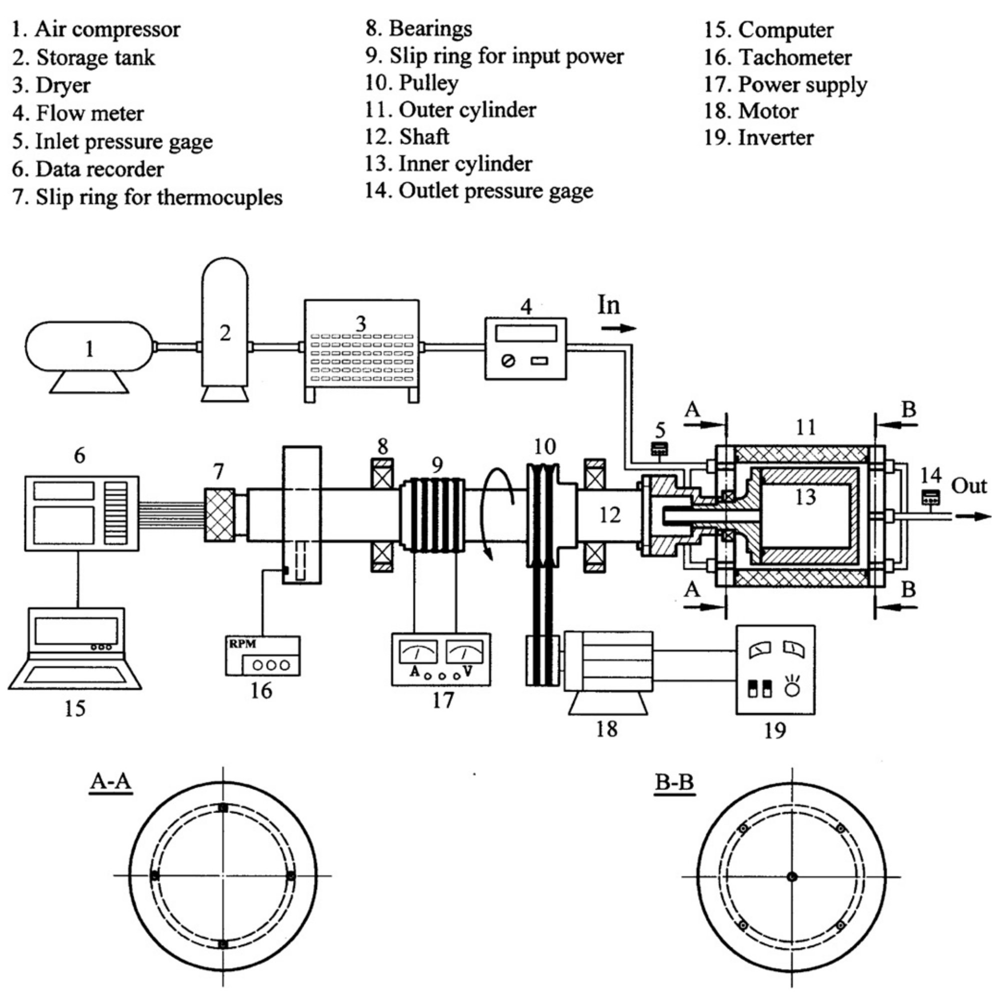

Fig. 1. Experiment setup.

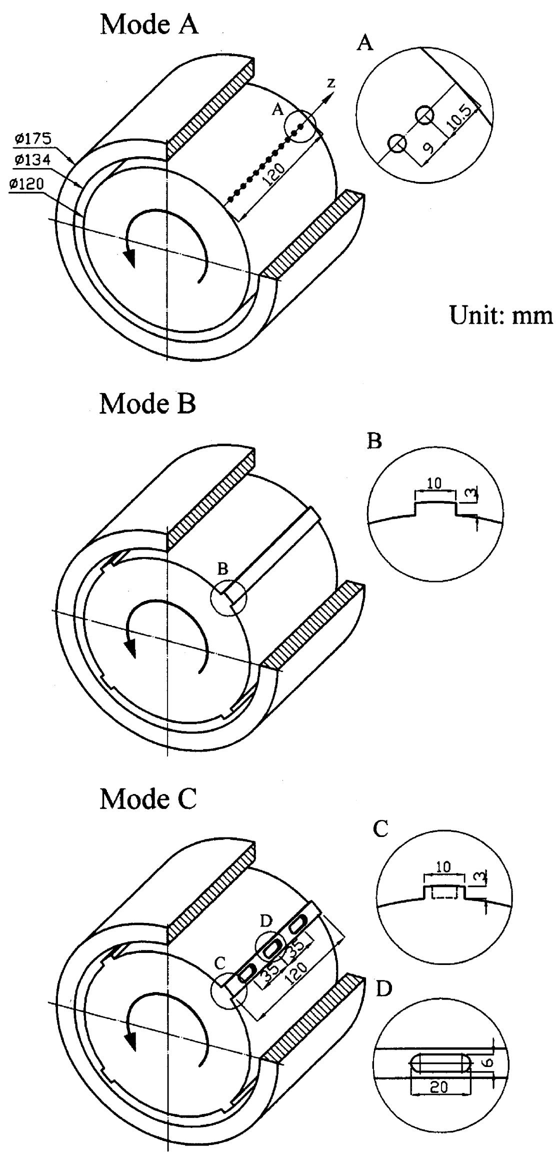

Fig. 2. Test section and detailed thermocouple positions.

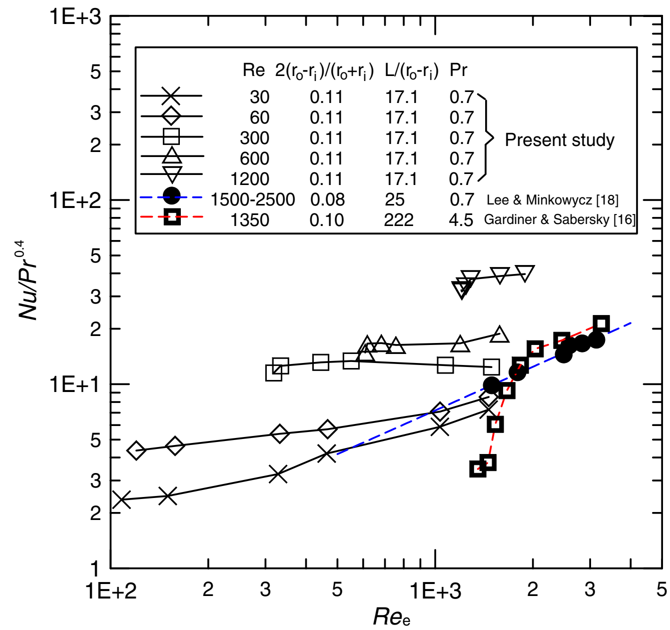

Fig. 3. Comparison with others' data for the system with smooth wall.

the inner cylinder. In mode C, three cavities were mounted on the top surface of each rib. Fig. 3 displays the dimensions of the ribs and the cavities and the positions of embedded TT-T-30SLE thermocouples. Twelve thermocouples were embedded in the inner cylinder with equal spacing in the axial direction. Three thermocouples were used to measure the ambient temperature, the air temperature at the channel inlet and the air temperature at the channel outlet. Five thermocouples were used to monitor the temperature on the outer surface of the outer housing. They were connected to a YOKOGAWA 2500E data recorder through the data slip ring and the passage in the inner cylinder and the rotating shaft. A film heater was attached to the outer surface of the inner cylinder. It was heated by a dc power supply through a brush and a power slip ring. The input power to the heater was determined as the product of the voltage and the current, read using a precision shunt resistor. The axial air flow was blown into the air tank by the air compressor. The air initially flowed through a filter to remove the oil, the water and the particles, then it entered the buffer chamber through the four inlet holes in the front shield before flowing into the annulus to carry the heat from the rotating inner cylinder, and finally impinged on the rear shield before running from the five outlet holes in the rear shield. The diameter of the inlet and outlet holes was 12.7 mm. Air flow rates of 11, 22, 111, 222 and 444 l/min were used in the tests, as determined by a flow meter. The system was assumed to be in the steady state when the temperature did not vary by more than 0.2 °C in 15 min. Pressure data were obtained at the channel inlet and the channel outlet using pressure transmitters.

3. Data reduction and uncertainty analysis

The measured fluid velocities, the rotational speeds and the pressure drops are used to determine the axial Reynolds numbers (Re), the rotational Reynolds numbers (Re_Ω) and the dimensionless pressure drops (P), using

$$Re = \frac{\rho V_a (r_o - r_i)}{\mu} \tag{2}$$

$$Re_\Omega = \frac{\rho (r_i \Omega)(r_o - r_i)}{\mu} \tag{3}$$

$$P = \frac{\Delta p}{0.5 \rho V_a^2} \tag{4}$$

where V_a represents the average velocity through the annular channel without ribs; r_o is the radius of the outer cylinder; r_i is the radius of the inner cylinder; Ω is the rotational speed of the inner cylinder, and Δp represents the pressure drop through the present system.

The local heat transfer coefficient (h) is evaluated as the ratio of the wall heat flux (q) to the difference between the local wall temperature (T_w) and the local coolant bulk temperature (T_b). The wall heat flux from (q) the outer surface of the inner cylinder to the flowing air is determined by subtracting the heat loss from the power supplied to the film heater. Ref. [20] presents the details of the heat loss test. The loss of the total input power is 6.3% in extreme cases. The fluid bulk temperature (T_b) can be determined by considering the local energy balance of input heat, estimated heat loss and the fluid enthalpy change. The annular channel is divided into 12 heating elements. The upstream bulk temperature of the first heating element is the measured inlet air temperature, and then the downstream bulk temperature can be evaluated by the method of the energy balance. Using the downstream bulk temperature of the previous heating element as the upstream bulk temperature of the following heating element, the bulk temperatures throughout the annular channel can be obtained. Finally, the Nusselt number is calculated by the following definition:

$$Nu = \frac{q(r_o - r_i)}{(T_w - T_b)k} \tag{5}$$

$$\overline{Nu} = \left(\sum_{i=1}^{12} (Nu\Delta z)_i \right) \Big/ L \tag{6}$$

The thermal conductivity (k) of air is based on the local bulk temperature; L is the length of the inner cylinder.

The maximum experimental uncertainty in the axial flow rate was around ±3.7% at 11 l/min. The rate of rotation was measured using a tachometer with some oscillation. The uncertainty in the rate of rotation was ±2.2%. The uncertainty in the pressure was ±6.4%. The errors in the temperature measurements were resulted from the inaccuracies in the recorder readings (about ±0.2 °C). Heat loss was responsible for an experimental uncertainty in the heat balance of ±6.5%. The analysis involved uncertainties in the thermophysical properties of air. Uncertainties in parameters were estimated using the root-sum-square method of Kline and McClintock [21] and Moffat [22]. The measured value and its uncertainty were given by $R = R \pm \delta R$. The uncertainties in the axial Reynolds number (Re), the rotational Reynolds number (Re_Ω), the dimensionless pressure drop (P) and the average Nusselt number ($\overline{Nu}$) were estimated to be ±4.4%, ±3.0%, ±7.5% and ±7.6%, respectively.

4. Results and discussion

In this work, the axial Reynolds numbers (Re) and the rotational Reynolds number (Re_Ω) vary from 30 to 1200 and from (zero OR 0) to 2922, respectively. Three modes of the inner cylinder without/with longitudinal ribs are tested. A series of experiments are conducted to determine the effects of Re, Re_Ω and test mode on the convective heat transfer of Taylor–Couette–Poiseuille flow in an annulus.

4.1. Experimental validation

Data concerning the system without ribs, obtained by Gardiner and Sabersky [16] and Lee and Minkowycz [18], are compared with the data herein to examine the validity of the present experiments. A description of the convective heat transfer based on effective velocity, provided by Gazley [23], is also employed. The effective velocity combines the average axial velocity (V_a) and the peripheral velocity ($r_i\Omega$) of the rotating inner cylinder and is expressed as

$$V_e = [V_a^2 + (r_i\Omega/2)^2]^{0.5} \tag{7}$$

The effective Reynolds number is given by

$$Re_e = \rho V_e (r_o - r_i)/\mu \tag{8}$$

Fig. 3 compares the results using the dimensionless parameter, $Nu/Pr^{0.4}$. As shown, the most of the data at $Re = 30$ and 60 lie on the curve extended from that fitted to the data presented by Lee and Minkowycz [18]. However, the data at $Re \geqslant 300$ clearly exceed those reported by Gardiner and Sabersky [16] and Lee and Minkowycz [18]. The dependence of $Nu/Pr^{0.4}$ on the Reynolds number at $Re \geqslant 300$ is much weaker than the values 0.5–0.8 as presented by Jakoby et al. [19]. The deviation is caused by the system configuration used herein. The system herein is not a typical one for solving the problem of Taylor–Couette–Poiseuille flow. It includes a specially designed entry and exit through which axial coolant flows (Fig. 2) for use in practical applications. The axial coolant initially enters the buffer chamber through four inlet holes in the front shield, before flowing into the annulus to carry the heat from the rotating inner cylinder, and finally impinges on the rear shield and runs away from five outlet holes in the rear shield. Therefore, the following types of fluid flow promote the heat transfer in the present system; (1) axial flow through the annular channel; (2) suddenly expanding flow at the outlet of the annular channel; (3) swirling flow near the rear shield and the rear part of the annular channel when the inner cylinder rotates; (4) Taylor–Couette flow in the annular channel when the rate of rotation of the inner cylinder exceeds a critical value. In a typical case, the heat transfer in the Taylor–Couette–Poiseuille flow is only affected by the axial flow and the Taylor–Couette flow. However, in real applications, such as the system herein, an additional complex flow caused by the rear shield must be considered.

4.2. Thermal behaviors in the stationary state

Fig. 4 presents the local Nusselt number (Nu_0) in the axial direction when the inner cylinder is stationary. The data indicate that the distributions of Nu_0 are generally smooth in the axial direction. This heat transfer characteristic differs from that associated with the channel flow, in which the local Nusselt number is typically maximal at the leading edge of the heating surface and slowly declines in the direction of the stream. The rear shield used herein is

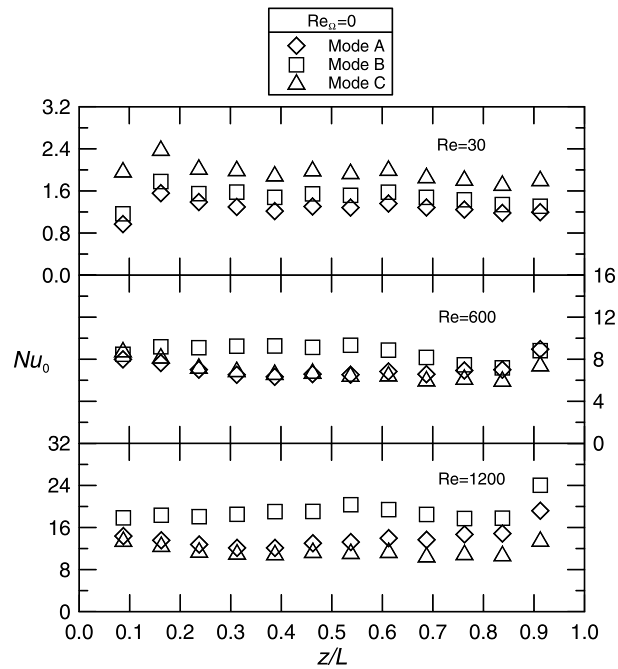

Fig. 4. The Nusselt number distributions in the axial direction for the inner cylinder in the stationary state.

responsible for this difference, as causes the impinging and suddenly expanding flow to promote the transfer of heat at the rear of the annular channel. Additionally, Nu_0 increases with the Re. Furthermore, the mounted ribs cause Nu_0 in mode B to exceed that in mode A. Nu_0 is best in mode C when Re is small (as at $Re = 30$) but is worst in mode C when Re is large (as at $Re = 600$ or 1200). Fig. 5 shows this result, by plotting the average Nusselt number ($\overline{Nu}_0$) as a

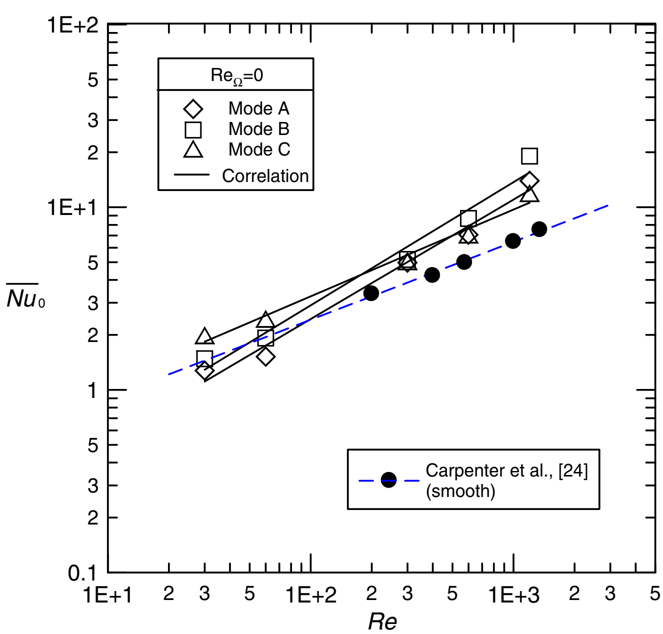

Fig. 5. Average Nusselt number as a function of axial Reynolds number for the inner cylinder in the stationary state.

Table 1
The corresponding factors of correlation on the Nusselt numbers without rotating

$\overline{Nu}_0 = mRe^n$, $30 \leqslant Re \leqslant 1200$			
	Mode A	Mode B	Mode C
m	0.12	0.13	0.36
n	0.65	0.68	0.48
rms (%)	2.2	3.3	1.2

function of the axial Reynolds number when the inner cylinder is stationary. This finding can be explained as follows. The system in mode C has ribs on the inner cylinder with three cavities in each rib. The cavities increase the effective surface to dissipate heat at small Re. However, at strong axial flow, heat accumulates in the cavities, reducing heat transfer. Fig. 5 also shows that $\overline{Nu}_0$ of the system herein exceeds that reported by Carpenter et al. [24] when Re exceeds about 200, because the impinging and suddenly expanding flow near the rear shield in the system herein. Finally, the measured data yield the following relationship between $\overline{Nu}_0$ and Re.

$$\overline{Nu}_0 = mRe^n \tag{9}$$

where m and n, presented in Table 1 for various test modes, are the corresponding factors in Eq. (9). The average deviation between the experimental data and those evaluated by Eq. (9) is under 4%. The range of application is $30 \leqslant Re \leqslant 1200$.

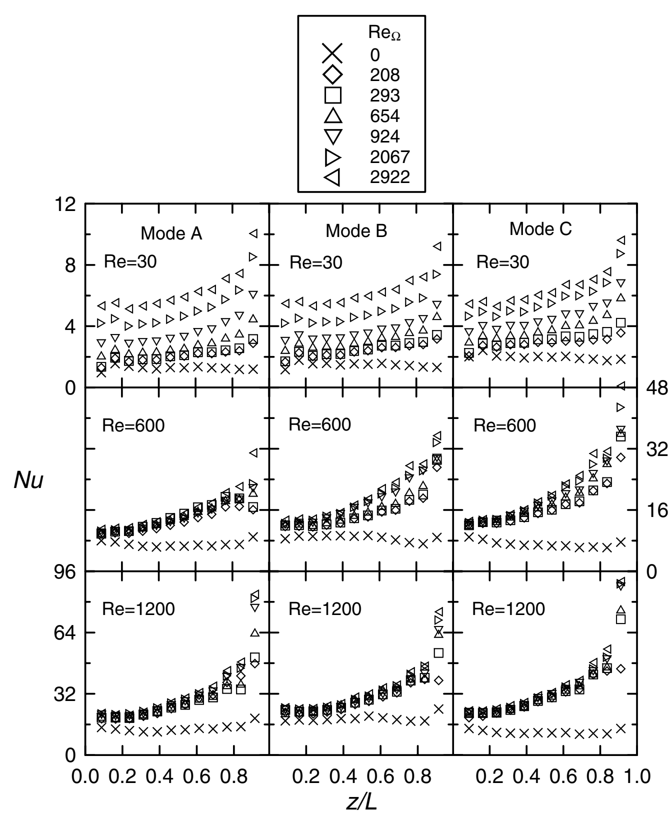

Fig. 6. The Nusselt number distributions in the axial direction for the inner cylinder in the rotating state.

4.3. Thermal behaviors in the rotating state

Fig. 6 plots the Nusselt number distributions (Nu) in the axial direction for a rotating inner cylinder. The data reveal that Nu is almost minimal at the inlet of the annular channel and rapidly increases in the axial direction. It differs greatly from that reported by Jakoby et al. [19], whose experimental findings showed that Nu is high in the inlet of the annular channel, and slowly falls along the axis until the thermal boundary layer is fully developed, and rises slightly because of the transition of the flow. The rear shield in the system herein explains the difference between the results herein and those in the literature [19]. The combination of the rear shield and the rotating inner cylinder is responsible for three fluid flow behaviors near the rear shield and the rear part of the annular channel: (1) the flow impingement on the rear shield; (2) the sudden expansion of the flow; (3) the swirl of the flow. These three fluid flow behaviors promote the dissipation of heat from the heated surface. Their impact is stronger further downstream in the annular channel. Fig. 6 plots the data obtained when the inner cylinder is stationary. The rotation clearly promotes the heat transfer. As aforementioned in Section 4.1, in the system herein, the rotation of the inner cylinder yields two types of flow; (1) swirling flow near the rear shield and the rear part of the annular channel; (2) Taylor–Couette flow in the annular channel. These two flows promote heat transfer, especially at the rear of the annular channel. Notably, in Fig. 6, Nu increases markedly with Re_Ω when Re is small (such as $Re = 30$). However, when Re becomes large (such as $Re = 600$ or 1200), the increased Re_Ω only slightly increases Nu, because the high flow rate in the axial direction prevented the Taylor vortex from appearing. Fig. 7 plots the $\overline{Nu}$ results obtained when the inner cylinder is rotating. The data demonstrate that $\overline{Nu}$ increases with Re. They also indicate that the $\overline{Nu}$ increases rapidly with the Re_Ω at low Re but less quickly at higher Re, revealing that the critical Taylor number, above which Nu increases rapidly, increases with Re. Fig. 7 also plots the relationship between $\overline{Nu}$ and Re_Ω at zero axial flow reported by Becker and Kaye [14] as the baseline.

4.4. Enhancing heat transfer

The ratio of $\overline{Nu}$ to $\overline{Nu}_0$ is introduced to elucidate the effect of Re_Ω on the enhancement in heat transfer. Fig. 8 plots $\overline{Nu}/\overline{Nu}_0$ as a function of Re_Ω. The results indicate that $\overline{Nu}/\overline{Nu}_0$ increases with Re_Ω and exceeds two at all Re and in

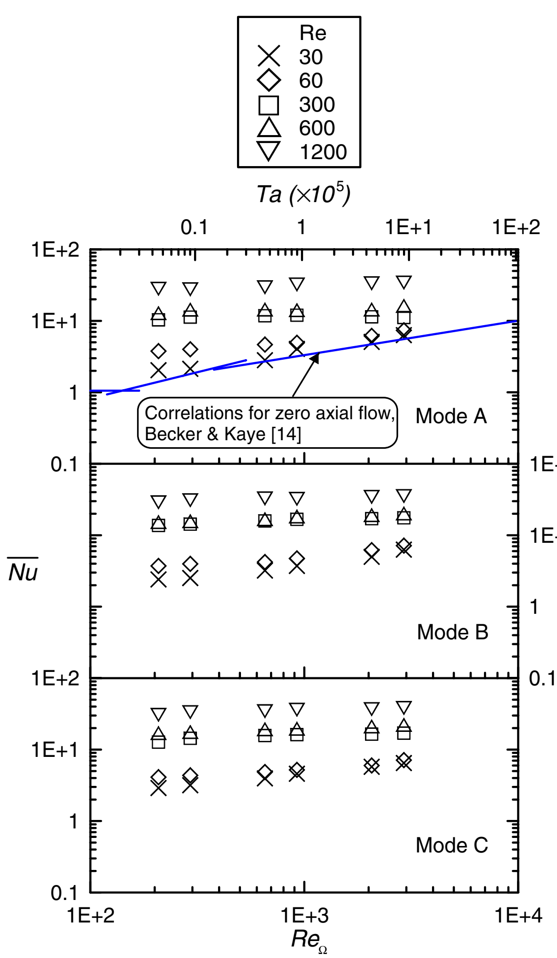

Fig. 7. Average Nusselt number results for the inner cylinder in the rotating state.

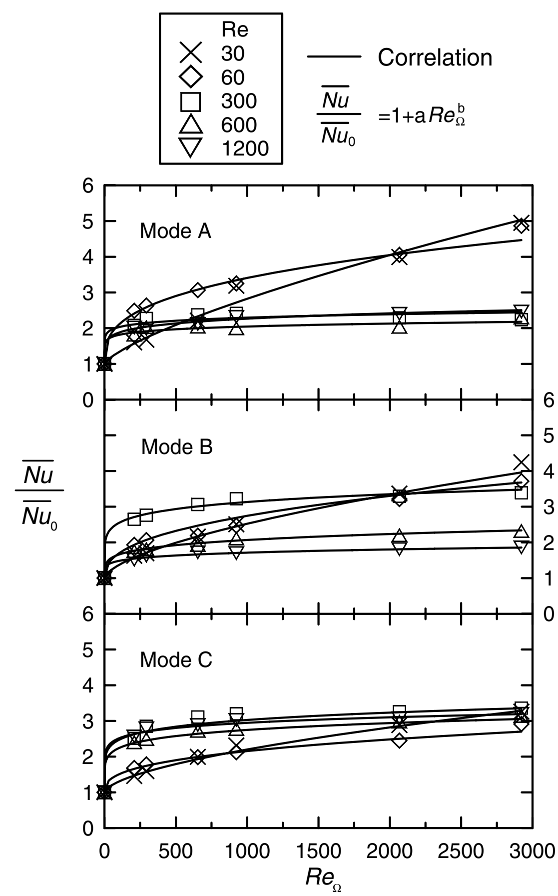

Fig. 8. Effect of rotational Reynolds number on the average heat transfer enhancements.

Table 2
The corresponding factors of correlation on the Nusselt number ratios with varying rotational Reynolds numbers

$\overline{Nu}/\overline{Nu}_0 = aRe_\Omega^b$, $Re_\Omega \leqslant 2922$

	Mode A					Mode B					Mode C				
	$Re = 30$	60	300	600	1200	$Re = 30$	60	300	600	1200	$Re = 30$	60	300	600	1200
a	0.011	0.23	0.65	0.49	0.42	0.021	0.11	0.81	0.25	0.22	0.019	0.096	0.77	0.62	0.91
b	0.74	0.34	0.10	0.11	0.16	0.62	0.40	0.14	0.21	0.17	0.60	0.36	0.14	0.15	0.11
rms (%)	2.00	0.36	0.94	0.99	0.26	0.34	1.07	0.18	0.16	0.38	0.40	0.37	0.57	0.02	0.18

all test modes. In this figure, open symbols represent the data; the lines through these symbols are least-square fits, and the basic correlation function is

$$\frac{\overline{Nu}}{\overline{Nu}_0} = 1 + aRe_\Omega^b \tag{10}$$

Table 2 presents the coefficients a and b at various Re and in various test modes. The average deviation between the experimental data and those obtained by Eq. (10) is less than 2%. The range of application is $Re_\Omega \leqslant 2922$. Notably, the dependence on Re_Ω (i.e. b in Eq. (10)) at $Re = 30$ ranges is given by $b = 0.6$–0.74, and at $Re = 60$, by $b = 0.34$–0.40, and at $Re = 300$–1200 by $b = 0.10$–0.21, indicating again that Nu increases rapidly with Re_Ω at low Re but less rapidly at higher Re. The effect of the test mode on heat transfer enhancement is now considered. $\overline{Nu}_A$ ($\overline{Nu}$ in mode A) is used as the baseline. The ratio of $\overline{Nu}$ to $\overline{Nu}_A$ is considered to investigate the effect of the test mode on the increase in heat transfer. Fig. 9 plots $\overline{Nu}/\overline{Nu}_A$ against Re_Ω. Mounting longitudinal ribs on the rotating inner cylinder normally increases heat transfer, especially at $Re = 300$ and 600. When $Re = 300$ or 600 and $Re_\Omega > 2000$, $\overline{Nu}$ of the system with ribs reaches around 1.4 times $\overline{Nu}_A$.

4.5. Heat transfer for at given pumping power constraint

Two important characteristics – heat transfer performance and pressure drop – are examined by performing experiments on fluid flow and heat transfer. The experimental results presented in the preceding sections clearly show that the heat transfer performance of the system with longitudinal ribs is better than that of the system without ribs. However, the ribs may obstruct the flow and increase the pressure drop in the annular channel. Therefore, more power is required to maintain the same flow rate as in the annular channel without ribs. Fig. 10 indicates that the dimensionless pressure drop (P) through the system herein declines as Re increases. Open symbols represent the data

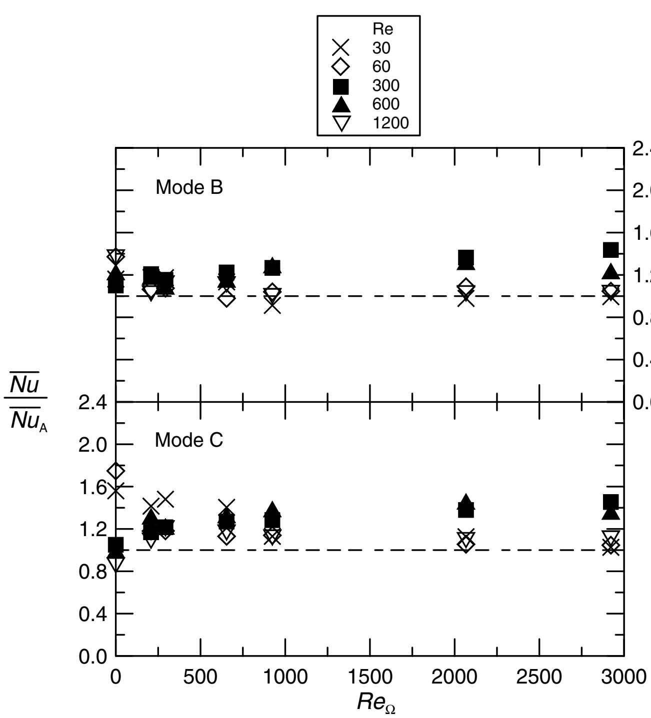

Fig. 9. Effect of test mode on the average heat transfer enhancements.

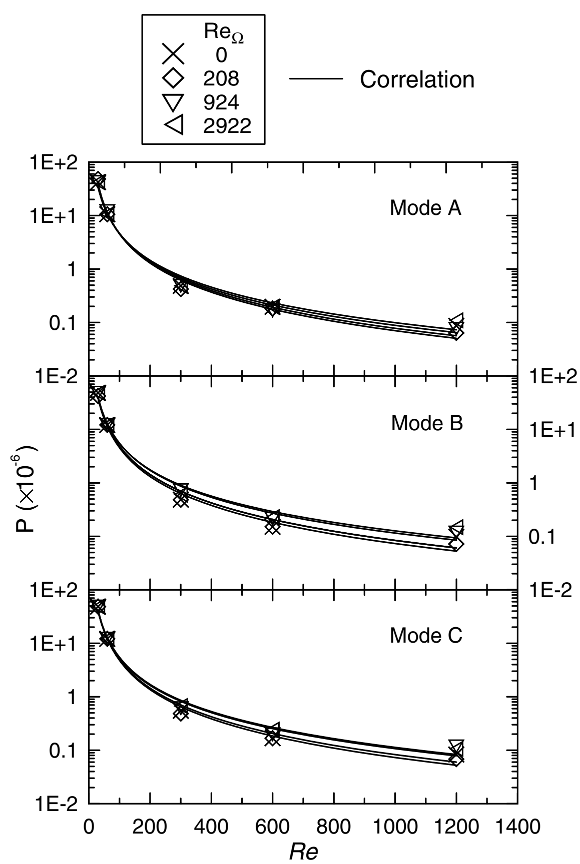

Fig. 10. Dimensionless pressure drop through different test modes.

Table 3
The corresponding factors of correlation on the dimensionless pressure drop with varying axial Reynolds numbers

$P = cRe^d$, $Re = 30$–1200

	Mode A				Mode B				Mode C			
	$Re_\Omega = 0$	208	924	2922	$Re_\Omega = 0$	208	924	2922	$Re_\Omega = 0$	208	924	2922
c	1.20e10	1.86e10	1.60e10	1.00e10	1.62e10	1.73e10	1.24e10	1.00e10	1.77e10	2.06e10	1.27e10	1.27e10
d	−1.71	−1.81	−1.77	−1.67	−1.76	−1.79	−1.68	−1.63	−1.78	−1.82	−1.69	−1.68
rms (%)	8.39	8.13	7.12	13.84	16.40	7.15	7.51	15.97	7.80	6.01	11.63	5.36

obtained for various Re_Ω and test modes; the lines that pass through these symbols are least-square fits, and the basic correlation function is

$$P = cRe^d \tag{11}$$

Table 3 lists the coefficients c and d for various Re_Ω and in various test modes. The average deviation between the experimental data and those obtained by Eq. (11) is approximately 9.6%. The range of application is $30 \leqslant Re \leqslant 1200$. Notably, the variations among the dimensionless pressure drops at various Re_Ω and in various test modes seem to be negligible, suggesting that most of the pressure drops are caused by the inlet and the outlet of the system. Additionally, a dimensionless pumping power (PRe^3) is introduced to determine the optimal test mode for high heat transfer. Fig. 11 plots the relationship between $\overline{Nu}$ and PRe^3 based on Eqs. (9)–(11). The results reveal that $\overline{Nu}$ increases with PRe^3 at various Re_Ω and in various test modes. The $\overline{Nu}$ also increases with Re_Ω. The figure shows an interest finding concerning the effect of the test mode on the heat transfer. The $\overline{Nu}$ of the system with ribs (modes B and C) usually exceeds that without ribs (mode A). However, the difference between the values of $\overline{Nu}$ in modes B and A slowly decrease as PRe^3 increases. Moreover, mode B (with ribs) is preferred for high heat transfer when $PRe^3 < 4.5 \times 10^{13}$ but mode C (with cavities on ribs) is the optimal configuration for high heat transfer when $PRe^3 > 4.5 \times 10^{13}$.

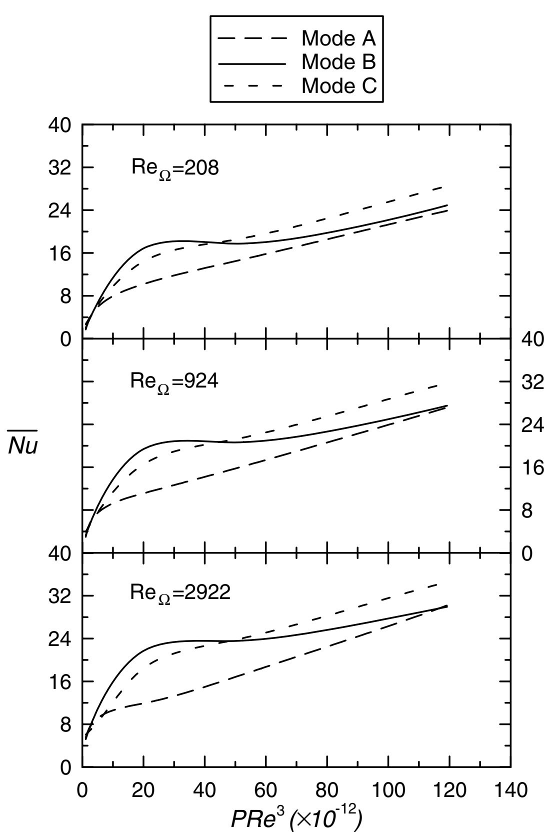

Fig. 11. Average Nusselt number as a function of dimensionless pumping power.

5. Conclusions

This work experimentally investigates the effects of the axial Reynolds numbers (Re), the rotational Reynolds number (Re_Ω) and the test mode on the convective heat transfer of the Taylor–Couette–Poiseuille flow in an annulus. Re and Re_Ω are varied from 30 to 1200 and from 0 to 2922, respectively. Three modes of the inner cylinder without/with longitudinal ribs are tested. The specially designed entry and exit of the axial coolant flow (Fig. 2) yield some interesting conclusions.

(1) The distributions of the Nusselt number (Nu_0) for a stationary inner cylinder are generally smooth along the axis in all test modes and all values of Re used herein. Additionally, Nu_0 increases with Re. The Nu_0 values of the system with ribs (mode B) exceed those without ribs (mode A). Among all test modes, the Nu_0 of the system with cavities on the ribs (mode C) is best at small Re (such as $Re = 30$ and 60) but is worst at large Re (such as $Re = 600$ and 1200).
(2) The Nusselt number (Nu) for the rotating inner cylinder is almost minimal at the inlet of the annular channel and then sharply rises in the axial direction. The average Nusselt number ($\overline{Nu}$) increases with Re. Nu increases rapidly with Re_Ω at low Re (as at $Re = 30$ and 60) but less rapidly at high Re (such as at $Re = 300$–1200).
(3) $\overline{Nu}/\overline{Nu}_0$ increases with Re_Ω and exceeds two for all values of Re and in all test modes. Mounting longitudinal ribs on the rotating inner cylinder typically promotes heat transfer, especially at $Re = 300$ and 600. When $Re = 300$ or 600 and $Re_\Omega > 2000$, $\overline{Nu}$ of the system with ribs reaches around 1.4 times $\overline{Nu}_A$.

(4) The inlet and outlet of the system are responsible for most of the pressure loss. For a given pumping power constraint (PRe^3), $\overline{Nu}$ of the system with ribs (modes B and C) normally exceeds that of the system without ribs (mode A). The difference between the values of $\overline{Nu}$ in modes B and A slowly decline as PRe^3 increases. Additionally, mode B (with ribs) is preferred to maximize heat transfer as $PRe^3 < 4.5 \times 10^{13}$ but mode C (with cavities on ribs) most promotes heat transfer when $PRe^3 > 4.5 \times 10^{13}$.

Acknowledgements

The authors would like to thank the National Science Council of the Republic of China for financially supporting this research under Contract No. NSC 93-2212-E-270-005.

References

[1] J.Y. Park, C.K. Choi, J.J. Kim, A study on dynamic separation of silica slurry using a rotating membrane filter: 1. Experiments and filtrate fluxes, J. Membr. Sci. 97 (1994) 263–273.
[2] P.J. Marto, Rotating heat pipes, in: D.E. Metzger, N.H. Afgan (Eds.), Heat and Mass Transfer in Rotating machinery, Hemisphere, Washington, DC, 1984, pp. 609–632.
[3] G. Baier, M.D. Graham, E.N. Lightfoot, Mass transport in a novel two-fluid Taylor vortex extractor, AIChE J. 46 (12) (2000) 2395–2407.
[4] Y.K. Yang, M.C. Jeng, Analysis of viscosity interaction on the misaligned conical–cylinderical bearing, Tribiol. Int. 37 (2004) 51–60.
[5] S.C. Tzeng, C.W. Lin, K.D. Huang, Heat transfer enhancement of nanofluids in rotary blade coupling of four-wheel-drive vehicles, Acta Mech. 179 (2005) 11–23.
[6] G.I. Taylor, Stability of viscous fluid between two rotating cylinders, Philos. Trans. Ser. A 223 (1923) 289–343.
[7] D. Coles, Transition in circular Couette flow, J. Fluid Mech. 21 (1965) 385–425.
[8] P.R. Fenstermacher, H.L. Swinney, J.P. Gollub, Dynamical instability and the transition to chaotic Taylor vortex flow, J. Fluid Mech. 94 (1979) 103–128.
[9] R.C. Diprima, H.L. Swinney, Instability and transition in flow between concentric rotating cylinders, in: H.L. Swinney, J.P. Gollub (Eds.), Hydrodynamic Instabilities and the Transition to Turbulence, Springer-Verlag, Berlin, Heidelberg, 1981, pp. 139–180.
[10] G.P. King, Y. Li, W. Lee, H.L. Swinney, P.S. Marcus, Wave speeds in wavy Taylor-vortex flow, J. Fluid Mech. 141 (1984) 365–390.
[11] K.N. Astill, Studies of the developing flow between concentric cylinders with the inner cylinder rotating, ASME J. Heat Transfer (1964) 383–392.
[12] K.W. Moser, L.G. Raguin, A. Harris, H.D. Morris, J. Georgiadis, M. Shannon, M. Philpott, Visualization of Taylor–Couette and spiral Poiseuille flows using a snapshot FLASH spatial tagging sequence, Magn. Reson. Imaging 18 (2000) 199–207.
[13] L.A. Bordag, O.G. Chkhetiani, M. Frőhner, V. Myrnyy, Interaction of a rotational motion and an axial flow in small geometries for a Taylor–Couette problem, J. Fluids Struct. 20 (2005) 621–641.
[14] K.M. Becker, J. Kaye, The influence of a radial temperature gradient on the instability of fluid flow in an annulus with an inner rotating cylinder, ASME J. Heat Transfer (1962) 106–110.
[15] T. Hayase, J.A.C. Humphrey, R. Greif, Numerical calculation of convective heat transfer between rotating coaxial cylinders with periodically embedded cavities, ASME J. Heat Transfer 114 (1992) 589–597.
[16] S.R.M. Gardiner, R.H. Sabersky, Heat transfer in an annular gap, Int. J. Heat Mass Transfer 21 (1978) 1459–1466.
[17] D.A. Simmers, J.E.R. Coney, A Reynolds analogy solution for the heat transfer characteristics of combined Taylor vortex and axial flows, Int. J. Heat Mass Transfer 22 (1979) 679–689.
[18] Y.N. Lee, W.J. Minkowycz, Heat transfer characteristics of the annulus of two-coaxial cylinders with one cylinder rotating, Int. J. Heat Mass Transfer 32 (1989) 711–722.
[19] R. Jakoby, S. Kim, S. Wittig, Correlations of the convection heat transfer in annular channels with rotating inner cylinder, ASME J. Eng. Gas Turbines Power 121 (1999) 670–677.
[20] G.J. Hwang, S.C. Tzeng, C.P. Mao, Heat transfer of compressed air flow in a spanwise rotating four-pass serpentine channel, ASME J. Heat Transfer 121 (1999) 583–591.
[21] S.J. Kline, F.A. Mcclintock, Describing uncertainties in single-sample experiments, Mech. Eng. (1953) 3–8.
[22] R.J. Moffat, Contributions to the theory of single-sample uncertainty analysis, ASME J. Fluids Eng. 104 (1986) 250–260.
[23] C. Gazley, Heat transfer characteristics of the rotation and axial flow between concentric cylinders, ASME J. Turbomach. 80 (1) (1958) 79–90.
[24] F.G. Carpenter, A.P. Colburn, E.M. Schoenborn, A. Wurster, Heat transfer and friction of water in an annular space, Trans. Am. Inst. Chem. Eng. 42 (1946) 165–187.